Drag coefficients in hydraulic channel

Student:

Samed Echi

Dissertation presented to the **Escola Supeior de Tecnologia e Gestão of the Instituto Politécnico de Bragança – Portugal**, to obtain the Master degree in Industrial Engineering - Mechanical Engineering, in the joint double diplomacy with the **Université Libre de Tunis - Tunisia**.

Advisors

Sérgio Manuel de Sousa Rosa

Yassine Ferchichi

Bragança

2020-2021

Acknowledgments

First and foremost, I am grateful to my supervisor Sérgio Rosa, not only for his huge help in this work but also for his inspiring, encouraging, and supporting personality. He was always willing to give me advice and guide me in my research. Working with him has been a great honor, and I will always consider myself lucky that I had him as an advisor. I am also very thankful to Amine Laarifi, for his kindness and exciting personality, I thank him for all the help and laboratory experience provided to the development of this work, he was always willing to help, give advice and share a laugh. Also, I am grateful to my supervisor Yassine Ferchichi for his valuable help.

Working in the LMFH lab has been a wonderful experience due to the great people in this laboratory. I am thankful to all the students that I worked with in the laboratory for making this research possible and for the great atmosphere that you created.

Of course, none of this could happen without the support and the unconditional love of my adorable family. I am grateful for my beloved mother Hasna, for giving me hope and filling me with strength in every step of this work, my great father Abdallahfor his trust, encouragement and advices in all the steps of my life, thank you for helping me to achieve my dreams.

Abstract

Experimental information is extremely useful in solving problems involving flow over bodies, as well as for determination of design parameters in aerodynamics and hydrodynamics, the drag coefficient being one of the most relevant as it allows to quantify the drag forces, that is, the total resistance of a body being dragged by a fluid. In this context, water tunnels have become indispensable research tools as they allow simulations involving all the complexity of a real flow in a fast and economical way, and together with experimental techniques of dimensional analysis, allow to standardize the coefficients in technical norms and with wide acceptance for different flow regimes and models of different geometric shapes, among which we can highlight the plates, bars, discs, cylinders, and hydrodynamic bodies. experimental tests were carried out to perform several measurements of hydrodynamic drag allowing a comparative study based on empirical drag coefficients in the literature for smooth cylinders,

Keywords: External flows, drag coefficient, water tunnel, cylindrical bodies and surface roughness.

Resumo

Informação experimental é extremamente útil para a resolução de problemas envolvendo fluxo sobre corpos, bem como para a determinação de parâmetros de projeto em aerodinâmica e hidrodinâmica, sendo o coeficiente de arrasto um dos mais relevantes, uma vez que permite quantificar as forças de arrasto, ou seja, a resistência total de qualquer corpo a ser arrastado por um fluido. Neste contexto, os túneis de água tornaram-se ferramentas de investigação indispensáveis, pois permitem simulações envolvendo toda a complexidade de um fluxo real de forma rápida e económica, e juntamente com técnicas experimentais de análise dimensional, permitem normalizar os coeficientes em normas técnicas com ampla aceitação para diferentes regimes de fluxo e modelos de diferentes formas geométricas, entre os quais podemos destacar as placas, barras, discos, cilindros e corpos hidrodinâmicos, todos com elevada aplicabilidade. Assim, neste trabalho, foram realizados ensaios experimentais para várias medições de arrasto hidrodinâmico, permitindo um estudo comparativo baseado em coeficientes de arrasto empíricos na literatura para cilindros lisos, e posterior comparação com diferentes graus de rugosidade no mesmo modelo. Consequentemente, foi também possível obter perceções sobre a viabilidade do equipamento, as suas principais limitações, bem como expandir e conciliar a teoria dos fluxos externos com a prática laboratorial.

Palavras-chave : Caudais externos, coeficiente de arrasto, túnel de vento, corpos cilíndricos e rugosidade superficial.

Summary

List of Figures

List of tables

Abbreviations and units:

Units and symbols	Abbreviation
μ[kg/m.s]	Dynamic viscosity
pT	Transport of quantities
τs	Strain rate
.ν[$m^2.s^{-1}$]	kinematic viscosity
ρ [kg/m^3]	Density
K	consistency index
N	fluid behaviour index
G	gravitational action
σ_{ij}	surface efforts.
F_R	resulting force
C_D	Drag coefficion
F_D	Drag force

CHAPTER 1

I. Introduction

I.1. Framework

There is a great deal of research in the area of fluid dynamics in the literature that attempts to develop and improve increasingly efficient machines, vehicles, power generation, and structures to improve comfort and convenience, and enhance the quality of life. Therefore, assuming that most of the elements in these fields involve mechanical stresses of elements immersed in fluids, establish parameters to group the associated properties, such as: velocity; density; viscosity; compressibility; body size and shape, to reduce the complexity of the equation, and reduce the cost by reducing the number of experiments. One of these parameters is the drag coefficient, which is the subject of this research.

The drag coefficient CD is a dimensionless number used in engineering to promote and quantify all the complex correlations of shape and flow conditions in external flow. These domains are established by the Reynolds number. The Reynolds number is another dimensionless parameter. Together with the drag coefficient, it provides a functional relationship. It allows a global understanding of the external flow phenomena from a single expression. It is itself based on the dimension analysis technology.

In the field of mechanical stresses, the boundary layer theory is a concept that provides a good understanding of the dynamics of forces flowing on the surface, mainly due to friction and pressure difference. However, this theory does not allow acceptable quantitative calculations without the help of experiments, especially in the case of highly applied circular elements, such as smooth and rough cylinders, which are strongly affected by the boundary layer failure phenomenon, resulting in increased strength due to the pressure gradient between the front and back surfaces immersed in the flow.

I.2. Contextualization

The importance of studying the flow of cylinders and cylindrical structures is due to their frequent use and applicability: tubes of heat exchangers, rain structures, pillars of bridges and towers which can have their useful life reduced under the action of wind, water or any other fluid interacting on its surfaces. In this context, there are hundreds of studies which support technical standards by semi-empirical methods where coefficients obtained in an experimental

way are used to determine drag forces for the purposes of design and design, for example.

II. Objectives

The primary objective in this work is to find drag coefficients for different surfaces, with different roughness, and different velocities, in hydraulic channel

The work will consist in calculation of drag coefficients in the hydraulic channel located at the Fluid Mechanics laboratory in ESTIG , in a general scope, to determine the hydrodynamic drag in the hydraulic channel from a model, in this case, of cylinders, bodies that present complex flow patterns, and as seen, extremely useful in engineering applications. To this end, laboratory experimentation was used to make it possible:

The experiments will be made for several geometries using water. To validate the procedures, simple geometries with drag coefficients well known and found in literature, will be used.

III. Work structure

This work is organized in the form of chapters. In chapter 1 we have an introduction to present the introductory aspects followed by the consolidation of the objectives. Chapter 2 consists of a theoretical foundation and an overview of fluid mechanics, where basic concepts are presented for understanding the dynamics of flows, forces, and the use of a water tunnel as a research instrument. Chapter 3 describes the methodology used to carry out the experimental activities, presentation of the steps, photos, relevant considerations, both for the test models and for the flow conditions. Chapter 4 presents the results obtained from the experimental tests, which in turn were validated and discussed through qualitative critical analysis and, where possible, quantitative. Finally, in chapter 5, the general conclusions of this work are presented in the light of the analysis of the results, main limitations, and a brief description about suggestions for future work and it’s structured in this way:

- Review the fundaments of external fluid flow
- Experiments in the hydraulic channel
- Thesis writing

CHAPTER 2

In this chapter we will do the bibliographic review including the fundaments of hydrodynamics, viscosity in Newtonian and Non-Newtonian fluids, then we will introduce the flow analysis and at last the drainage of submerged bodies

I. Bibliographic Review /Fundamentals Of Hydrodynamics

This chapter consists of the theoretical foundation from a previous presentation of the concept of viscous fluids and properties to the general principles of hydrodynamics: science responsible for studying the movement in practically incompressible fluids, being, therefore, a starting point for understanding the flows.

I.1. Viscosity in Newtonian fluids

Despite the variety of definitions found in the literature, fluids can basically be defined as substances presented in liquid or gaseous form, which, once subjected to a minimum tangential force, flow according to the figure 1. Another remarkably more elementary definition says that these substances do not have their own physical form and when they occupy a container, they end up taking their characteristic form.

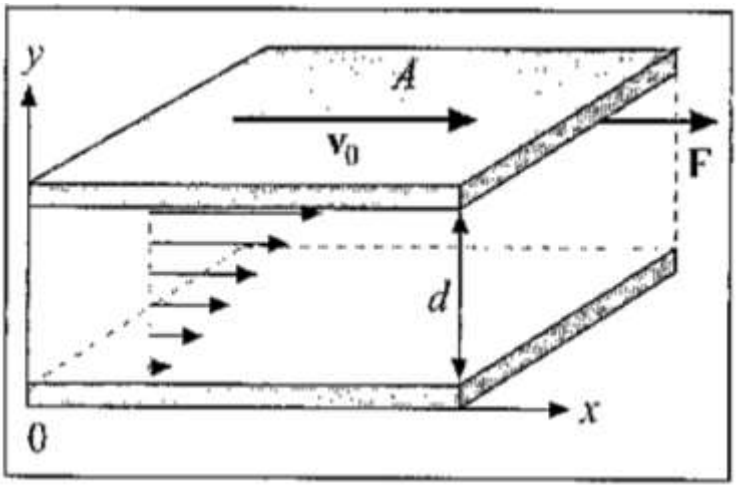

Figure 1. Reaction to tangential stress applied between parallel plates [1].

The quick visualization of the figure allows verifying the fluid response by applying the tangential effort, a force in the opposite direction, the cutting effort, associated with a

deformation rate du/dy of the speed profile. The shear force acting on an element of the fluid area produces shear stresses in it, which immediately allows us to contextualize the concept of Newtonian fluid $v_0(y)\tau$.

Newtonian fluids such as water, air and oil are those whose behavior obeys Newton's Law of Viscosity and, therefore, ensures that the commitment between the shear stress and the referred strain rate is a linear relationship that physically corresponds the dynamic viscosity in the international system.

$$\tau = \mu \frac{du}{dy} \tag{1}$$

The viscosity it is a particular property of each substance and varies for the same fluid according to other properties that describe its thermodynamic state, mainly pressure and temperature, independent variables that are normally related by state equations. Properties already mentioned such as strain rate, velocity and acceleration deal specifically with the description of the movement, while viscosity itself fits into the transport of quantities pT.

$$\mu = \mu_1(p, T) \tag{2}$$

In gases and most liquids, viscosity increases slowly with pressure, while an increase in temperature causes a decrease in viscosity in liquids and an increase in viscosity in gases. In terms of temperature, such behaviors justified through microscopic analysis as temperature variations significantly influence the cohesion forces and kinetic friction between fluid molecules [1]. Visually, highly viscous fluids are sticky and difficult to flow, as the difficulty in sliding the fluid layers caused by intermolecular interactions results in increased resistance to shear stresses. The effects of pressure, in turn, are moderate in relation to viscosity [2].

For convenience, viscosity can also be written in terms of kinematic viscosity, by the relation with fluid density, a characteristic that measures the degree of concentration of its mass in a given occupied volume. On the assumption that the fluid is a continuous and homogeneous medium, the density is given by the relationship described below.

$$\rho = \frac{m}{V} \rightarrow \rho_1(p, T) \tag{3}$$

In gases, this property becomes quite variable with temperature and increases almost proportionally with pressure, which can be easily found in thermodynamic tables in the specialized literature. [2; 3]. As for liquids, which are denser than gases at atmospheric pressure, a reasonable increase in pressure does not significantly affect the value of their density, which for practical purposes is considered constant and characterizes the flow as approximately incompressible.

Table 1. Physical properties of common fluids at pressure and 1 atm20 ºC [2].

Fluid	Dynamic Viscosity $\mu\ [kg/m.s]$	Kinematic Viscosity $\nu\ [m^2.s^{-1}]$	Density $\rho\ [kg/m^3]$
Air	$1{,}8\ x\ 10^{-5}$	$1{,}50\ x\ 10^{-5}$	1,2
Gasoline	$2{,}9\ x\ 10^{-4}$	$4{,}22\ x\ 10^{-7}$	680
Water	$1{,}0\ x\ 10^{-3}$	$1{,}01\ x\ 10^{-6}$	998
Ethyl alcohol	$1{,}2\ x\ 10^{-3}$	$1{,}52\ x\ 10^{-6}$	789
SAE 30 oil	0,29	$3{,}25\ x\ 10^{-4}$	891
Glycerin	1,5	$1{,}18\ x\ 10^{-3}$	1260

The viscosity of Newtonian fluids can be determined by means of equipment suitable for this purpose, viscometers and rheometers. At a specific temperature, viscometers are usually based on the relationship between the resistance force in the direction of the fluid movement and its velocity, or on friction along the walls of the viscometer, generally classified into three types: tube, sphere and rotary.

Tube viscometers are based on the time a given fluid flows through a capillary tubing, the most commonly used are U-shaped capillaries or Ostwald viscometers. In the viscometer of the figure 2, cavities are used with marks to time the pour time under the influence of gravity from one mark to another. Depending on the duration, its viscosity will be higher or lower, being proportional to the time used.

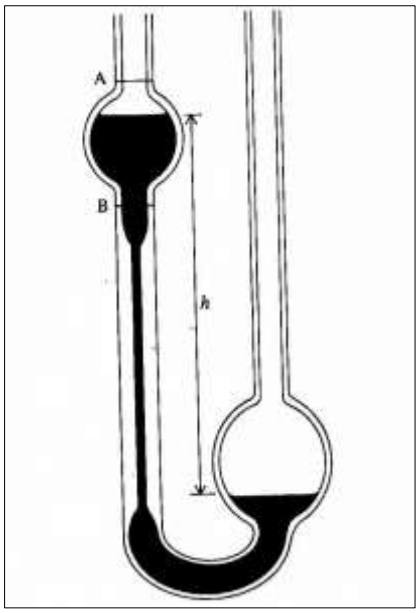

Figure 2. Ostwald viscometer: the main bulb, with the A and B level marks [4].

It is noticed that the experimental test requires a stopwatch and thermometer to determine the temperature that influences the viscosity, determined by equation 4, Hagen's Law - Poiseuille applied in a capillary tube of constant area, length and total radius through the pressure difference Δp [5]. Once the pour time is known the average speed can be replaced by

$$\bar{u} = L/t$$

$$\mu = \frac{\Delta p R^2}{8L\bar{u}} = \frac{\rho g h R^2}{8L\bar{u}} = \frac{\rho g h R^2}{8L^2} t \tag{4}$$

A sphere viscometer consists of a vertical or inclined pipe in which a sphere of radius falls under gravitational action. In this experiment, viscosity is determined based on the terminal velocity reached when the force in the direction of motion (vertical drag) equals the gravitational force (downward). Starting from this velocity, size and specific mass of the sphere and the liquid along with Stokes' Law, it is possible to determine the fluid viscosity according to the equation 5.

$$\mu = \frac{2}{9} \frac{(\rho_s - \rho_f)}{\bar{u}} g R^2 \tag{5}$$

The third classification covers rotary viscometers, those most suitable for viscosity estimation in non-Newtonian fluids. The working principle is to cause a rotation with the aid of a body, normally cylinders and cones, together with the confined fluid. The configuration of the rotation viscometer between concentric cylinders, known as Couette flow is one of the most used in this

classification, and knowing the resulting torque for different angular velocities, it is possible to construct shear stress curves by strain rate.

I.2. Introduction to non-Newtonian fluids

The so-called non-Newtonian fluids are those whose shear stress is not directly proportional to the strain rate. In this context, there is an effort to propose empirical equations that model this behavior, usually the exponential model, which is the behavior index of a flow, and a consistency index nk [6].

$$\tau = k \left(\frac{du}{dy}\right)^n \tag{6}$$

$$k \left|\frac{du}{dy}\right|^{n-1} \frac{du}{dy} = \eta \frac{du}{dy} \tag{7}$$

The equation 7 is usually used to represent the apparent viscosity, depending on the deformation rate and similar in shape to ηequation 1, for the case where Newtonian viscosity is applied. Through these models, the figure 3 for graphical comparison of the rheological behavior of fluids. Both graphs are related by the slope of the curves, since it is the apparent viscosity itself at a given point.

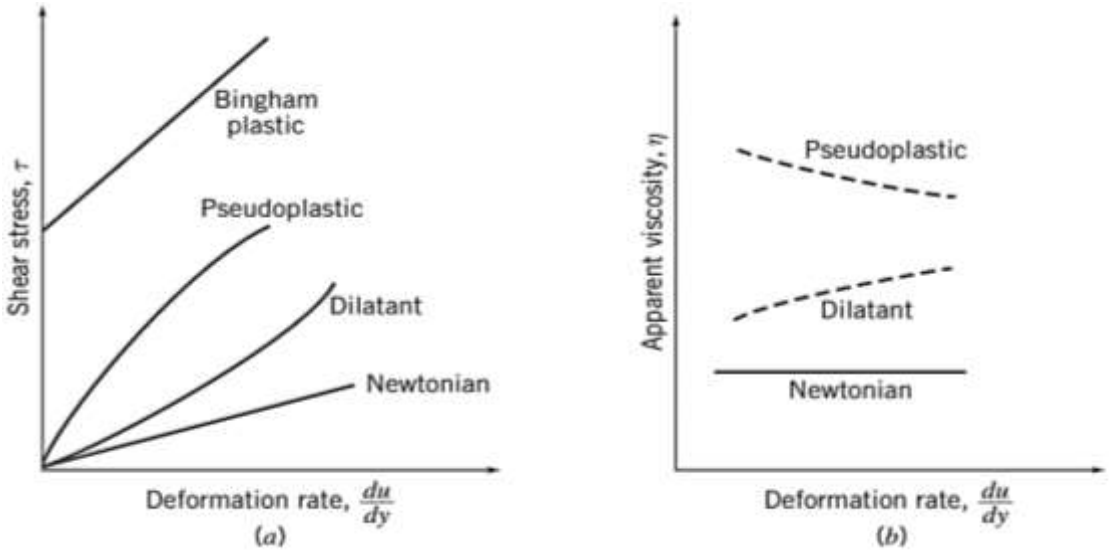

Figure 3. Rheological behavior for various fluids [6].

Pseudo-plastic fluids are those that present, that is, the apparent viscosity decreases with the

increase of the strain rate, becoming less viscous when subjected to shear stresses. Prime examples include polymer solutions, and some inks. In the opposite situation, when the apparent viscosity increases with the increase of the deformation rate, there are expanders such as starch solutions and sand in suspension $\eta < 1 \eta > 1$.

The so-called Bingham plastics are non-Newtonian fluids with a preliminary behavior of a solid material; however, they show to deform continuously once the shear stress increases and exceeds a certain limit, then starts to flow. Typical examples of these fluids are toothpastes, drilling mud and clay suspensions.

The study of non-Newtonian fluids enters the field of rheology and becomes even more complicated in cases where the apparent viscosity may be dependent on the time of deformation. In this context, rheometers have become appropriate equipment for the study of non-Newtonian fluids. There are several types available on the market, among which the rotational (or torque), capillary and extensional ones stand out, depending on the purpose and how the tension is applied [5].

Rotational systems are based on the rotation of a cylindrical, conical or circular body immersed in the fluid experiencing a viscous drag force when a rotation is imposed. The working principle of a capillary system consists of collecting a sample and forcing it to extrude under high pressure through a cylinder or die. This pressure drop then measured by a transducer to provide the pressure flow rate for determining apparent viscosity.

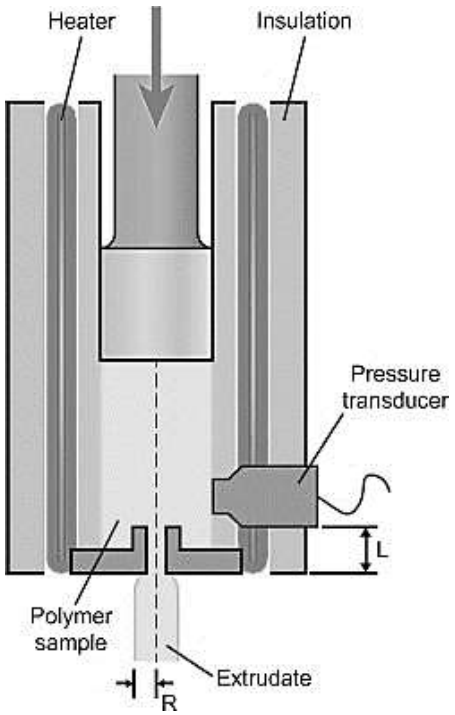

Figure 4. Schematic of a modern capillary rheometer with temperature control [7].

Modern rheometers such as the one in figure 4 allow the in-depth study of the rheological properties of fluids, obtaining stress-by-strain rate curves under specific temperature conditions. They are more expensive than viscometers with the advantage of allowing analysis as a function of deformation time.

I.3. Flow analysis

First, the analysis in fluid mechanics starts from the previous characterization of the flow regime. Although there are different ways of classification, in viscous fluids the characterization is dependent on variations in the physical properties of the flow, as shown in the scheme of figure 5.

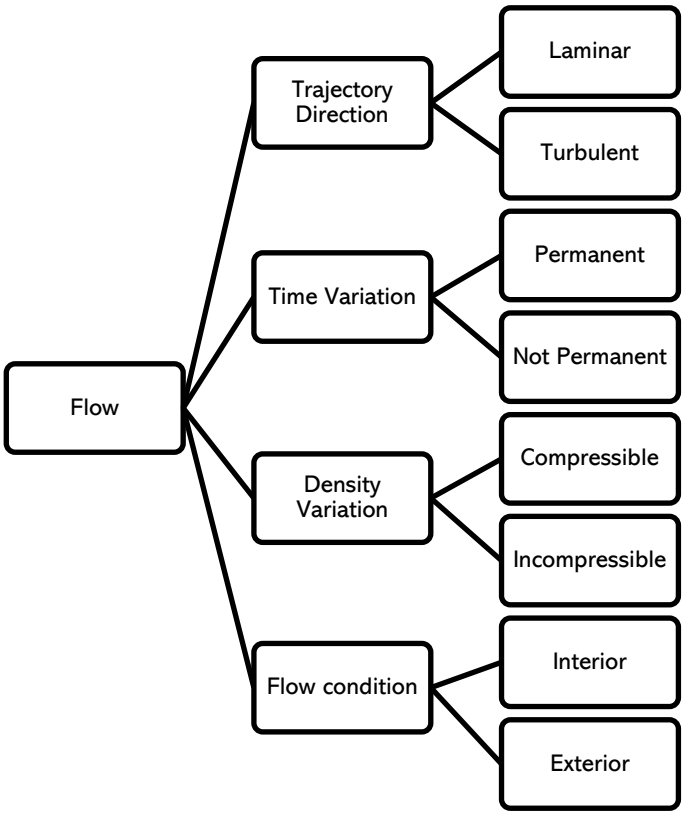

Figure 5. Preliminary flow characterization [3.8].

The main parameter that allows the characterization of flow under velocity V and length scale Lin viscous fluids is the Reynolds number Re. This is the main dimensionless parameter that introduces the theoretical separation between laminar and turbulent flows and a transition region.

$$Re = \frac{\rho VL}{\mu} = \frac{VL}{\nu} \quad (8)$$

The laminar flow regime is less common in practice and is characterized by the highly ordered movement of fluid layers, such as highly viscous fluids such as oils flowing at low speeds. On the contrary, turbulent flow, more common in everyday engineering applications, is observed for randomness and high velocity fluctuations, as occurs in the flow of low viscosity fluids such as air, at high speeds.[9].

Steady state is one in which the physical properties of the fluid can be variable from point to point under the condition that they do not change over time. This condition implies that the configuration of the properties at any time remains the same [3], and when this does not occur we have a non-permanent underflow.

In certain flows, when there are significant variations in volume with pressure, it is important to consider the effects of compressibility, especially in gas flows above or close to the speed of sound. The dimensionless parameter that establishes a theoretical separation between gas flows is the Mach number Ma, and therefore, when this value is less than 0.3, the flow is considered incompressible [2]. Although no fluid is theoretically incompressible, this can be considered in the flow of many liquids because in this case, density variations are insignificant with pressure variations [9].

In the classification when the condition, the fact is taken into account and the fluid is flowing in a confined space, the condition of interior flow, as occurs in industrial pipelines or is still flowing freely over a surface, as in the case of submarines, planes and cars. In the latter, they differ from the former in that viscous effects are relevant in a boundary layer region much closer to the surface of the body or object [6].

Given the above classifications, the analysis of the flows itself consists of using a mathematical model that models the flow and takes place with the aid of computational methods, through integral or differential analysis. Integral analysis, also known as control volume analysis, consists of limiting a finite region of the domain by performing balances of incoming and outgoing flows, determining global effects. The differential approach, or dimensional analysis, in turn focuses on describing the details of each coordinate of the vector field.

By intercepting the mentioned techniques, we have the full filament of the basic laws of physics: the principle of conservation of mass and linear momentum, in addition to an equation of thermodynamic state. The general law of conservation of mass expressed by the equation 6, says that the rate of change over time of mass within a volume added to the total mass flow in terms of the difference between the flow into and out of the control surface must be nil.

$$\int_{VC} \frac{d\rho}{dt}\, dV + \int_{SC} \rho\, \vec{V}\,.\vec{n}\, dA = 0 \tag{9}$$

There are different ways to find the solution to the mass conservation equation, one of the most viable being the application of the divergence theorem, or Gauss' theorem, which allows writing the equations 7 and 8they being the equation of continuity in compressible and incompressible form, respectively. In both, the speed is considered $\vec{V}$a three-dimensional vector of components u, v and w.

$$\frac{d\rho}{dt} + \vec{\nabla}\,.\left(\rho\vec{V}\right) = 0 \tag{10}$$

$$\vec{\nabla}.\vec{V} = \frac{du}{dx} + \frac{dv}{dy} + \frac{dw}{dz} = 0 \tag{11}$$

As in the previous case, the direct application of the Reynolds transport theorem facilitates obtaining the general equation for the conservation of momentum in a control volume, a principle that can also be verified by Newton's law when a volume element dV of mass, undergoes gravitational action and surface efforts.

$$\sum \vec{F} = \int_{VC} \rho\vec{g}\, dV + \int_{SC} \sigma_{ij}\,.\vec{n}\, dA = \int_{VC} \frac{d}{dt}\,(\rho\vec{V})\, dV + \int_{SC} \left(\rho\vec{V}\right)\vec{V}\,.\vec{n}\, dA \tag{12}$$

Briefly, the equation 9it states that the net force acting on the control volume is given by the rate at which the variation of the moment within the volume occurs plus the variation of the rate of the moment in terms of what leaves and enters across the boundaries of that same control volume. By applying the divergence theorem, the equation 10, namely, the differential equation of conservation of the Cauchy moment.

$$\frac{d}{dt}\,\rho\vec{V} + \vec{\nabla}\,.\left(\rho\vec{V}\vec{V}\right) = \rho\vec{g} + \vec{\nabla}\,.\sigma_{ij} \tag{13}$$

Cauchy's equation becomes useful when the tension tensor is established σ_{ij} which act on volume. Under simplified conditions, as in the case of liquid flow, which in turn are considered

incompressible, the tensor is defined as the sum of the normal or hydrostatic pressure with the viscous stresses. In the case of compressible fluid flow it is the thermodynamic pressure related to a state function

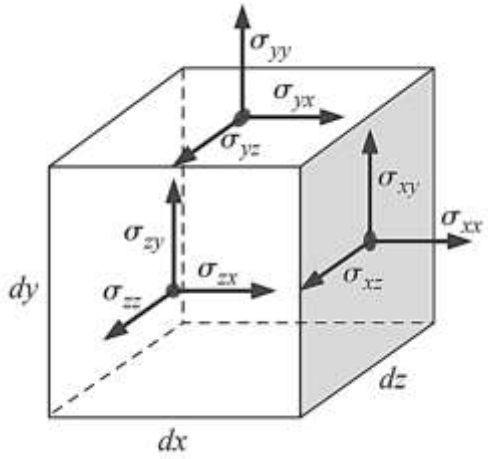

Figure 6. Stress Tensor Components in a Control Volume [3].

Limiting itself to the case of incompressible flow of Newtonian fluids and under isothermal conditions, the viscous stress tensor is linearly proportional to the strain rate tensor, and, therefore, the stress tensor is completely established and applied in the Cauchy vector equation to obtain the general form of the equation of motion, the ε_{ij} equation 11 of Navier-Stokes, also expressed in terms of its coordinates, and, with the aid of the incompressible continuity equation xyz:

$$\rho \frac{d\vec{V}}{dt} = -\vec{\nabla}P + \rho\vec{g} + \mu\vec{\nabla}^2\vec{V} \tag{14}$$

$$\rho\left(\frac{\partial u}{\partial t} + u\frac{\partial u}{\partial x} + v\frac{\partial u}{\partial y} + w\frac{\partial u}{\partial z}\right) = -\frac{\partial P}{\partial x} + \rho g_x + \mu\left(\frac{\partial^2 u}{\partial x^2} + \frac{\partial^2 u}{\partial y^2} + \frac{\partial^2 u}{\partial z^2}\right) \tag{15}$$

$$\rho\left(\frac{\partial v}{\partial t} + u\frac{\partial v}{\partial x} + v\frac{\partial v}{\partial y} + w\frac{\partial v}{\partial z}\right) = -\frac{\partial P}{\partial x} + \rho g_y + \mu\left(\frac{\partial^2 v}{\partial x^2} + \frac{\partial^2 v}{\partial y^2} + \frac{\partial^2 v}{\partial z^2}\right) \tag{16}$$

$$\rho\left(\frac{\partial w}{\partial t} + u\frac{\partial w}{\partial x} + v\frac{\partial w}{\partial y} + w\frac{\partial w}{\partial z}\right) = -\frac{\partial P}{\partial x} + \rho g_z + \mu\left(\frac{\partial^2 w}{\partial x^2} + \frac{\partial^2 w}{\partial y^2} + \frac{\partial^2 w}{\partial z^2}\right) \tag{17}$$

Because the equations are highly complex, dimensional homogeneity of variables, properly the dimensional analysis. Basically, the technique guarantees a functional relationship, obtained by experimental data, between the so-called dimensionless groups enabling practical, economical and realistic solutions to problems with many variables. Thus, the technique will be contextualized in a practical way in the study of submerged bodies.

I.4. Drainage of submerged bodies

The configuration in which there is relative movement between immersed bodies and viscous fluids is called external flow. These flows are unconfined and are characterized by the presence of a thin region in which the flow is disturbed by the presence of the body, the boundary layer, and another in which the viscosity effect is negligible and the fluid can be treated as non-viscous [10].

In the first region, the boundary layer theory appears as an alternative for understanding and solving problems involving viscous flows since it would be impossible to apply the Navier-Stokes equation to the complete flow field. In this sense, the boundary layer flow can be laminar (LTB) or turbulent (TLB) with several factors that affect the transition (T) in relation to the stagnation point, which highlights the adverse pressure gradient, the surface roughness, heat transfer, field forces and free current disturbances [6].

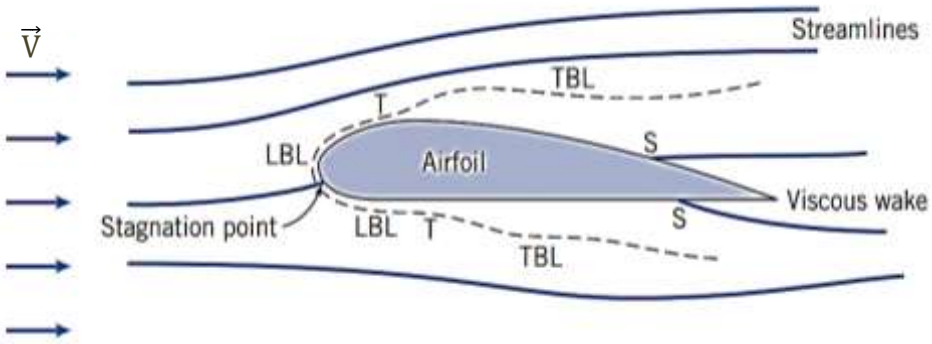

Figure 7. Illustration of the airfoil boundary layer in an outer flow [6].

In the region of the boundary layer, the movement causes a net force F_D, hydrodynamics for liquids or aerodynamics for air. In normal flows to a long body with a constant cross section, called two-dimensional, the resulting force is a reaction obtained by the integration of the distribution of shear forces and pressure along the surface.

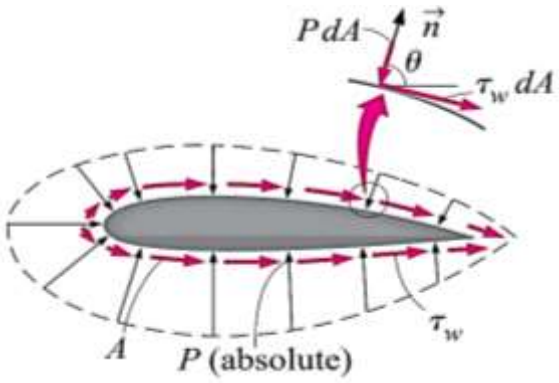

Figure 8. Aerodynamic force and its components [3].

The vector composition of the force is given by the resistance component in the normal flow direction, the support F_L, and other in the parallel direction, and the drag. However, because of the integration on the area element $F_D dA$ not being a practical means of resolution, dimensional analysis and experimentation are commonly used to obtain them.

$$F_L = -\int_A (-P \sin\theta + \tau_w \cos\theta)\, dA \tag{18}$$

$$F_D = \int_A (-P \cos\theta + \tau_w \sin\theta)\, dA \tag{19}$$

One of the main conveniences of dimensional analysis in the context of external flows enters at this point: to practically determine the resistance of a long body, knowing that in advance, the resulting force is dependent on physical variables of the flow [11], as evidenced in equation 13.

$$\begin{aligned} F_R &= g(\rho, V, L, \mu) \\ g_1(F_R, \rho, V, L, \mu) &= 0 \end{aligned} \tag{20}$$

Essentially, dimensional analysis seeks to reduce variables (in this case) using compaction techniques and grouping them in a dimensionless form using the theorem $N = 5$ of Pi Buckingham, which reduces the problem into dimensional variables.K

Commonly,$K = 3$, because the fundamental dimensions are the mass, length, and time and by them all the others are written. Thus, it is assumed that the other physical variables are represented by mlt specific mass, velocity, and fluid viscosity $mllt^{-1}ml^{-1}t^{-1}$. When choosing variables like, and, in this case, the theorem guarantees at least two dimensionless and dependent parameters through a function.

$$g_2(\Pi_1, \Pi_2) = 0 \tag{21}$$

$$\Pi_1 = F_R \rho^d V^b L^e = (ml^{-3})^d (lt^{-1})^b (l)^e (mlt^{-2})$$
$$\Pi_2 = \rho\, V^h L^i \mu^j = (ml^{-3})^d (lt^{-1})^h (l)^i (ml^{-1}t^{-1})^j$$

The technique unfolds in the proper equation of the fundamental dimensions, and obeying the condition that the exponent of the dimensionless is null. In this sense, so that and, are dimensionless, the equation leads to the value of the exponent , and Under these conditions, Pi Buckingham's theorem supports the functional relationship between the dimensionless, showing the coefficient of the resulting force as dependent on the Reynolds number of the flow.$\Pi_1 \Pi_2 d = -1b = -2e = -2h = 1i = 1j = -1 C_R Re$

$$g_2\left(\frac{F_R}{\rho\, V^2 L^2}, \frac{\rho V L}{\mu}\right) = 0$$
$$C_R = f(Re) \tag{22}$$

The result proposed by equation 19it is the most convenient and generic way of dealing with the problem of obtaining hydrodynamic forces in external flows. Theoretically the relationship still shows the dimensionless of force expressing the relationship between the resulting force and the dynamic force, expressed by the equation 20, and the relationship between the ratio between inertial and viscous forces that allows us to identify whether the behavior is laminar or turbulent Re[11;12].

$$C_R = \frac{F_R}{\frac{1}{2}\rho\, V^2 A} \tag{23}$$

In general, the above relationships are valid for incompressible flow $(Ma < 0.3)$on any body, and for practical purposes, it takes into account the shape, presence of surface roughness$(\epsilon)$and orientation of it in relation to the flow to then establish the characteristic length of the Reynolds number and the area$(\alpha)A$. Therefore, in general terms, the relations below apply to obtain the dimensionless force coefficients.

$$C_L = f(Re, Ma, \varepsilon, \alpha) \tag{24}$$

$$C_D = f(Re, Ma, \varepsilon, \alpha) \tag{25}$$

With the example of the drag coefficient, the equation 23 shows part of it due to shear stresses caused by surface-fluid friction and the other due to pressure, also called shape drag, which occurs mainly due to the pressure difference between the front and rear faces of a body. In reality, these effects rarely occur at the same time and usually one effect is preponderant [8; 10]. Friction drag is generally negligible for a flat surface perpendicular to the flow and has a maximum value for when it is parallel to it, as in the case of flat plates. In the latter, the phenomenon of boundary layer separation does not occur and the drag is entirely due to friction.

$$C_D = \frac{F_{D;friction}}{\frac{1}{2}\rho V^2 A} + \frac{F_{D;pressure}}{\frac{1}{2}\rho V^2 A} = \frac{F_D}{\frac{1}{2}\rho V^2 A} \tag{26}$$

Figure 9, presents the drag force comparisons for different bodies and the presence of a separate region of the flow, a viscous mat with recirculating flow and low pressure. The so-called separation point marks the disruption of the boundary layer by a deceleration of fluid particles in response to an adverse pressure gradient. It is observed that, in general, the larger the separated region, the greater the contribution of pressure drag, usually predominant in bodies with large curvatures (blunt).

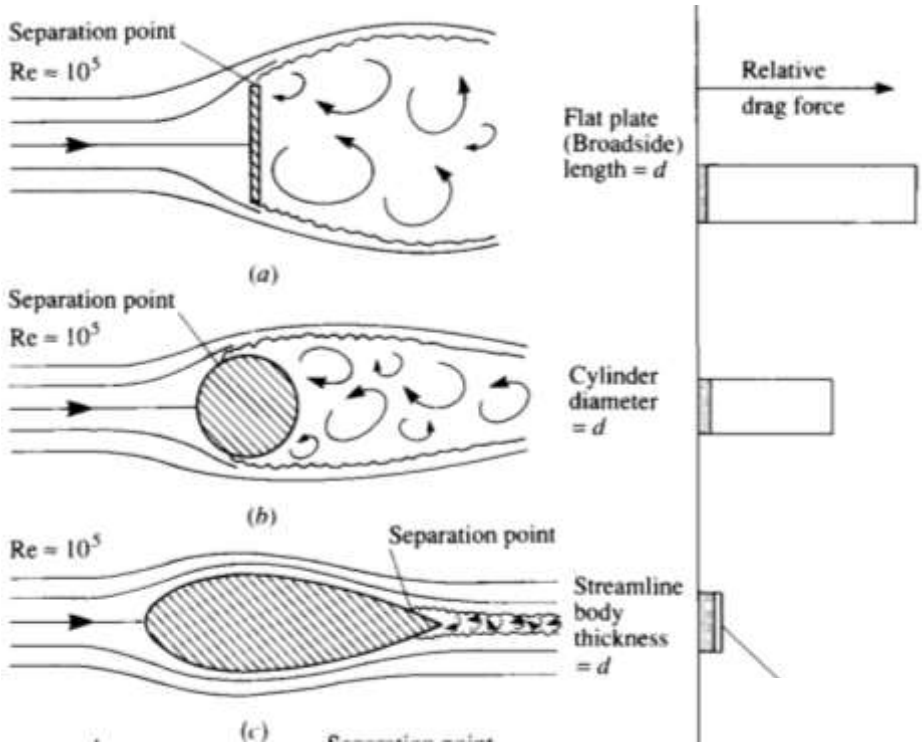

Figure 9. Natures of the drag force. [11].

The typical graph of the drag coefficient of a blunt body is presented in figure 10for the case of a smooth cylinder of characteristic length equal to the diameter. Experimentally, different behaviors can be observed according to the Reynolds interval, with emphasis on the constant interval between, the presence of the laminar boundary layer when, the turbulent layer above this value, and the drag crisis, characterizing the flow transition region.$10^3 < Re < 10^5 Re \lesssim 2\ x\ 10^5$.

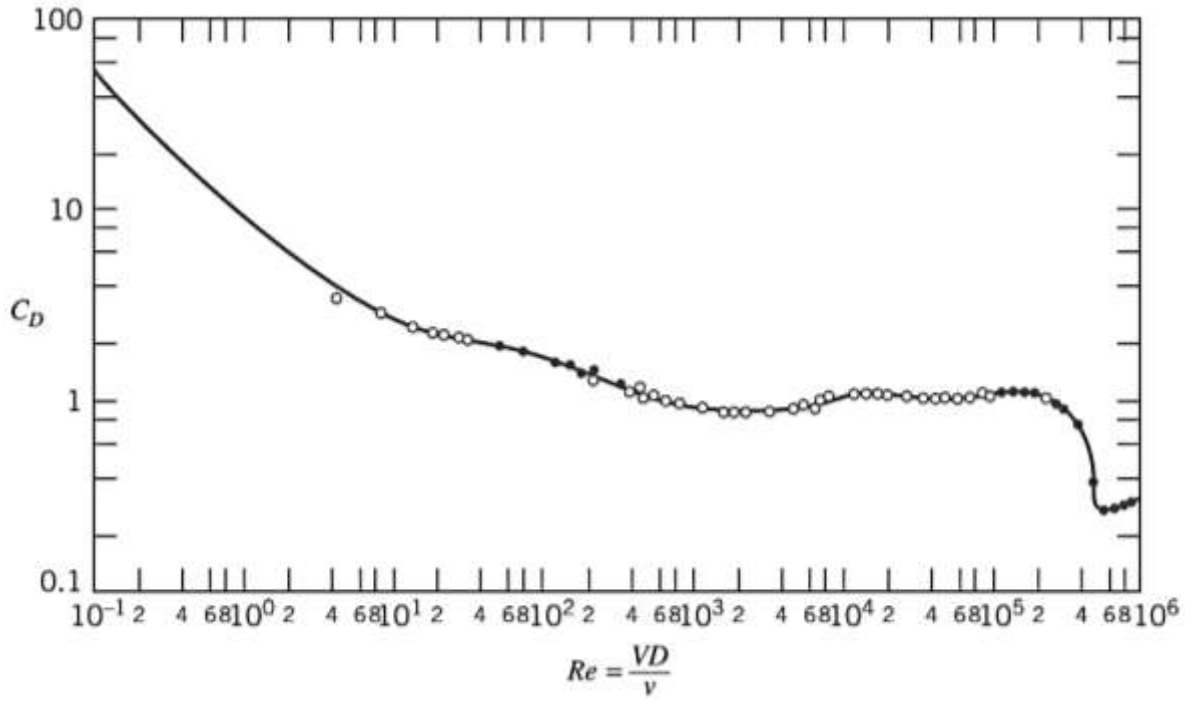

Figure 10. Cylinder drag coefficient in cross flow. [6].

The drag coefficient crisis seen in these flows is due to the transition of the boundary layer, which becomes turbulent, moving the separation point to a downstream point on the surface [3]. This displacement is perceived by the reduction in the size of the rear conveyor and the reduction of the preponderant pressure drag.

In cylinders, the separation of the boundary layer occurs at an angle of approximately from the stagnation point to the laminar boundary layer, and about in the turbulent layer (stickier) and this phenomenon may also be influenced by the insertion of turbulence [2; 3; 8]. The induction of turbulence results in the anticipation of the drag crisis at a lower Reynolds number than would occur if it were smooth.

In smooth spheres, the variation of the drag coefficient shows the same characteristics in relation to cylinders. However, it is noteworthy that under slow flow conditions in which the fluid is evenly distributed around the body, it was observed that the drag coefficient varies linearly with the Reynolds number, leading to$Re \lesssim 1$equation 25 - Stokes' law.

$$C_D = \frac{24}{Re} \tag{27}$$

$$F_D = 3\pi\mu VD \tag{28}$$

Relatively to other common bodies, experimental studies reveal that the drag coefficient is dependent on the Reynolds number, mainly in values below, and above these, tend to be relatively constant. As this last situation is quite every day in the engineering context, the way to obtain agile solutions is by consulting the drag coefficients in technical norms or standardized tables, widely available in the literature.$Re = 10^4$[11]for bodies such as plates, bars, cubes, disks, cylinders, spheres, cones and ellipsoids.

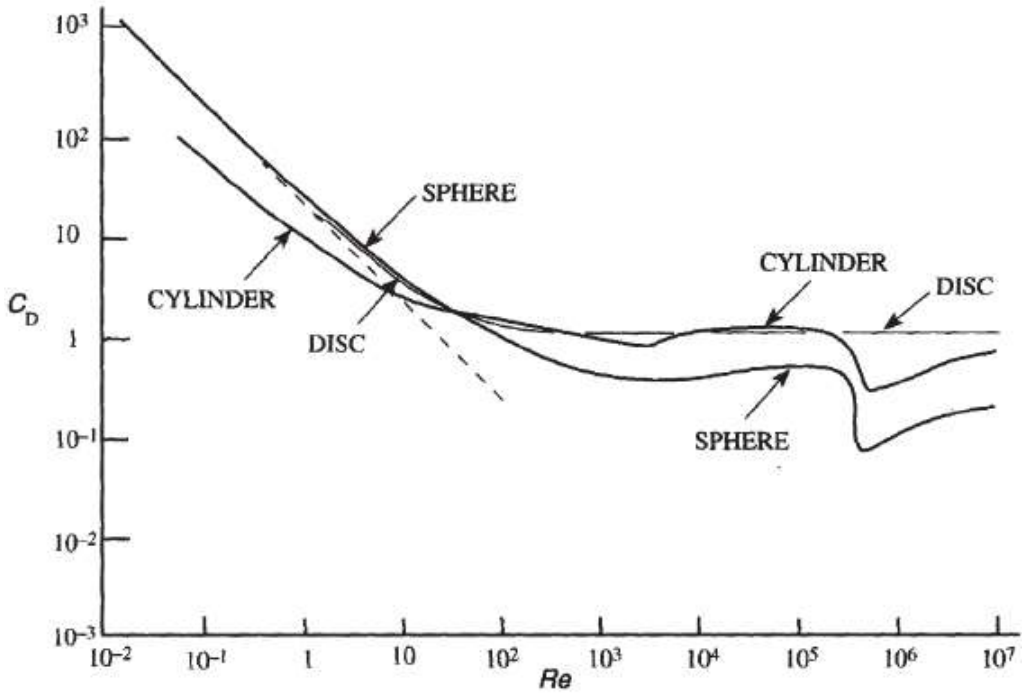

Figure 11. Drag coefficients of common (smooth) bodies. [11].

I.5. Hydraulic channel

The practical experimentation in hydraulic channels essentially consists of a simulation in open channels, which are characterized by being a free surface flow found in nature or in engineering structures. In nature, calm flows can be observed in large rivers near their estuaries, while turbulent ones can be found in Mountain Rivers, for example [13].

In structures, open channels can be for irrigation water supply, basic sanitation, etc., or even specifically designed for studies. In this sense, hydraulic channels have become one of the resources widely used in the understanding of external flows, as they model the actual flow behavior, in addition to enabling measurements of hydrodynamic forces through a measurement system.

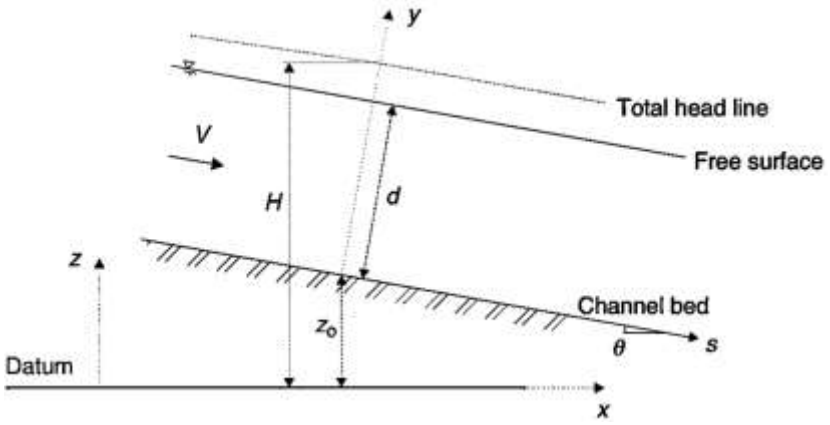

Figure 12. Free channel flow scheme [13].

The main working fluid in a hydraulic channel is water, and the resource consists of a long channel made of transparent material (figure 13) and a closed circuit fed from a reservoir with the aid of hydraulic pumps. In general, the simplest structures are composed of elements such as control valves and lifting system for studies under different inclinations [13; 14].

The figure 13 shows a schematic example of a Company Gunt - Equipment for Engineering Education laboratory hydraulic channel, model HM 150.21 used for student purposes whose elements are described below. Note the presence of the transparent test section along its length where, for the study of hydrodynamic forces, a body fixation system must be configured to obtain the forces acting on the external flow.

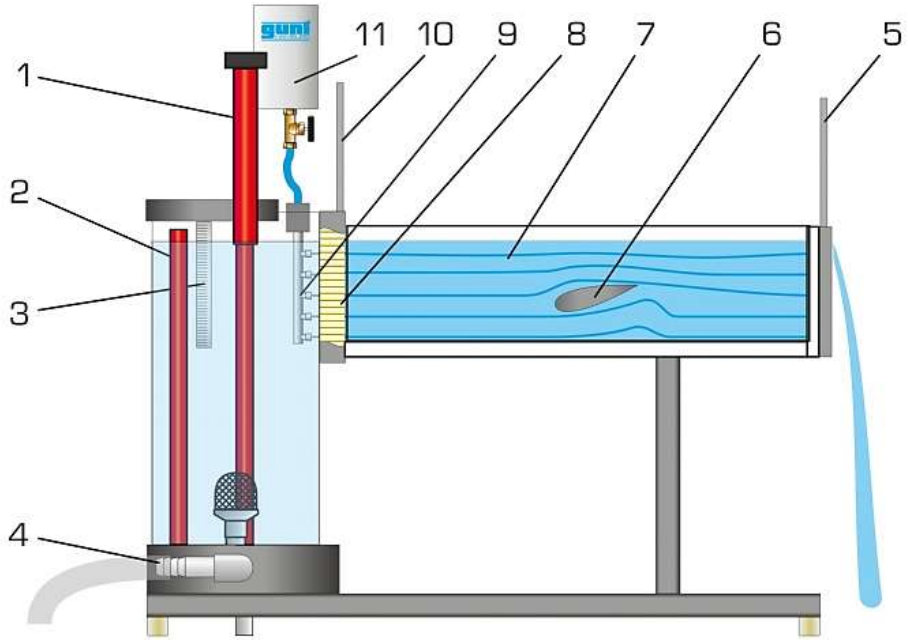

Figure 13. Hydraulic laboratory experimentation channel [15].

Where, 1. Adjustable overflow; 2. Tank; 3. Scale; 4. Water supply; 5. Weir at the water outlet; 6. Body; 7. Experimental flume; 8. Flow straightener; 9. Distributor for contrast medium; 10. Sluice gate at the water inlet to the experimental flume; 11. Tank for contrast medium.

CHAPTER 3

In this chapter we will introduce the water tunnel and its characteristics as well as the geometry we will use which is the cylinder, the different roughness's we will use and the measurement machine that we managed to construct after doing its technical drawing using SolidWorks then we will describe the whole process

I. Materials

This chapter describes the equipment and materials used to perform the tests, its limitations, and the results obtained.

To perform the experimental tests, various materials and equipment were used from the beginning of this phase until the results were obtained, in order to ensure that the experiments were standardized and the results were reliable.

I.1. Hydraulic channel

The main equipment that allowed the tests to be performed was the hydraulic channel. This is located in the fluid mechanics laboratory of the Polytechnic Institute of Bragança.

This equipment was manufactured by Engineering Laboratory Design Inc. with a power of 0,56 kW and a channel length of 2,20 meters. It also has a system for regulating the inclination.

Figure 14. Hydraulic channel in the fluid mechanics laboratory at IPB.

I.2. Cylindrical extension

This acrylic extension is part of the hydraulic channel accessories supplied by the manufacturer. It has an internal diameter of 7,5 cm and a length of 10 cm.

Figure 15. Cylindrical extension.

I.3. Flow Calculation

The process for performing an experimental flow calculation is to restrict the cross section of the hydraulic channel in order to allow the installation of a duct that permits the fluid to be directed into an external container.

Figure 16. Equipment and methods for experimental flow calculation.

The time spent from the time the duct was directed into the container until it was removed was measured with the use of a timer. The exterior container, on the other hand, lacked a scale to determine the volume. As a result, the volume would be determined using the difference in container mass before and after the fluid was introduced.

Figure 17. Mass of the empty container.

After performing the previous procedure, you can see the mass of the container with the fluid in Figure 18.

Figure 18. Mass of container with water.

You can determine the flow rate using the following expression if you know the particular mass of the water, the mass difference, and the time it takes to fill the container:

$$Q = \frac{m_f - m_0}{\rho\, \Delta t} \tag{29}$$

To calculate the fluid velocity in the section restricted by the acrylic extension, the following expression is used:

$$v = \frac{Q}{\pi\, {r_s}^2} \tag{30}$$

All the values used and obtained are shown in Table 2:

Table 2. Parameters of the experimental tests.

Description	Symbol	Valor
Initial mass of the container	m_O	1,45 kg
Final mass of the container	mf	30,30 kg
Specific mass of water	ρ	997 kg/m³
Time measured on the stopwatch	Δt	8,36 s
Flow rate	$\dot{Q}$	0,0034 m³/s
Section Radius	r_s	0,0375 m
Fluid velocity at the section	v	0,78 m/s

Figure 19. The configuration of the water tunnel and the slope that defines the velocity.

I.4. Abrasive sheets and it's equivalent roughness

Table 3. Selection of abrasive sheets for surface coating [21].

Abrasive Files	
Commercial name (grain)	**Absolute roughness ε**
P320	$0{,}046\ mm$
P120	$0{,}125\ mm$
P80	$0{,}210\ mm$
P40	$0{,}425\ mm$

.

Figure 20. Abrasive sheet P320.

Figure 21. Abrasive sheet P120.

Figure 22. Abrasive sheet P80.

Figure 23. Abrasive sheet P40.

II. Methodology process

In order to prevent the geometry to move with the flow a measurement base system was built in heavy material so the base couldn't move even with high velocity rate, and also using screws to fix the base to the body of the water tunnel and having an axe at the center where we fix our stick that we will use as the center of the cylinder as shown below.

Figure 24 and 25 show the measurement base system designed in SolidWorks and built-in steel, purposely for this study.

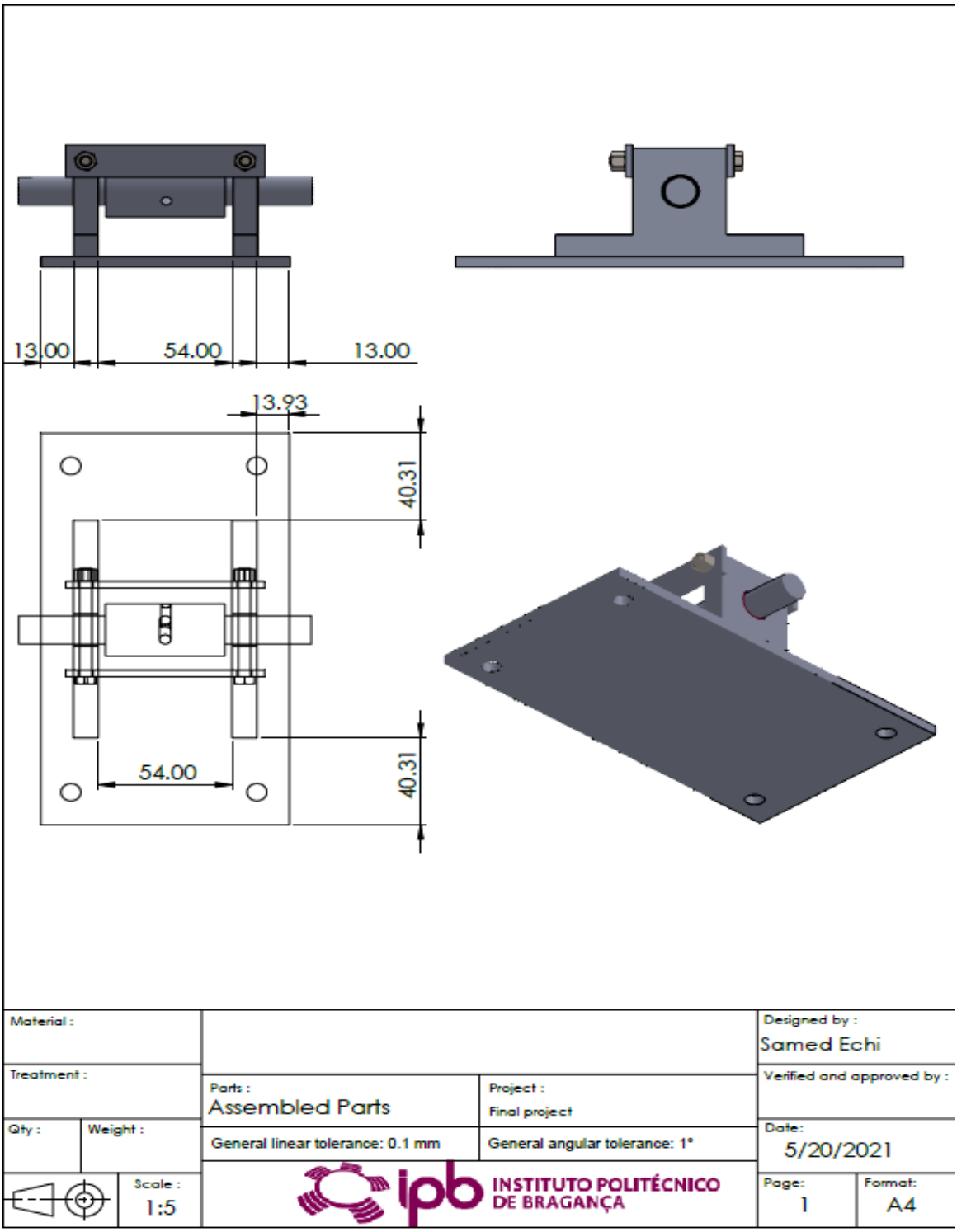

Figure 24. The measurement system.

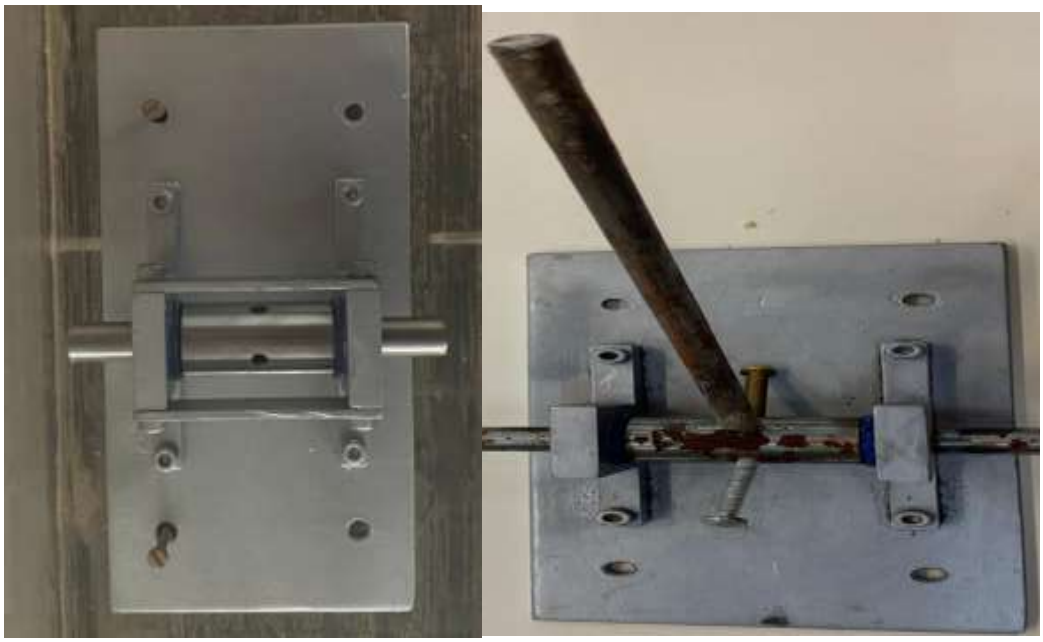

Figure 25. Base measurement machine with and without the stick that holds the cylinder.

Figure 26. The process of measuring the drag coefficient.

The water comes out of the pump through the hydraulic channel until it reaches the measuring machine which is fixed with screws. The water drags the cylinder and to maintain its position we had to attach a wire from the cylinder to the beginning of the water tunnel where we hang a weight to balance the force made by the water, as shown in Figure 27.

Figure 27. Attached weight.

Then taking the weights and measuring it as shown below.

Figure 28. Measuring the weight.

Figures 29 to 32 show the positioning of each cylinder to be studied.

Figure 29. Simulation for cylinder with roughness 1.

Figure 30. Simulation for cylinder with roughness 2.

Figure 31. Simulation for cylinder with roughness 3.

Figure 32. Simulation for cylinder with roughness 4.

CHAPTER 4

In this chapter we will present the results of the experiments detailed in tables and graphs.

Results and Discussion

This chapter presents and analyze the experimental data. Due to the model and the equipment, we used we could only have five velocities that allows us to drown the cylinder.

Table 4. Slope and its equivalent velocity.

Slope (°)	Velocity(m/s)	Flow(m^3/s)	Flow height(cm)	Channel area(m^2)
0	0.085	0.0034	26.8	0.04
2.5	0.087	0.0034	26	0.039
5	0.092	0.0034	24.6	0.0369
7.5	0.094	0.0034	24	0.036
10	0.1	0.0034	22.5	0.0337

For each velocity we got a different drag force, which was given by the mass weight ($F_D = m\ g$).

For the 5 different surfaces we got the flowing drag forces:

Table 5. The velocity and drag force for all surfaces.

	Commercial name (Grain)			
Velocity (m/s)	P320	P120	P40	P80
0.085	11.772E-3	49.05E-3	64.746E-3	0.049
0.087	34.335E-3	57.879E-3	68.67E-3	0.042
0.092	47.088E-3	51.993E-3	83.385E-3	0.06174
0.094	75E-3	87E-3	90.E-3	0.06272
0.1	100.062E-3	104.967E-3	103.986E-3	0.1078

The drag coefficient C_D was then obtained by the theoretical equation $F_D = \frac{1}{2} C_D\ \rho A V^2$, where ρ is the specific weight of water, A is the frontal area of the geometry, and V the velocity of the water.

Table 6. Drag coefficient low roughness surfaces.

	Commercial name	
Velocity (m/s)	**P320**	**P120**
0.085	1.08	4.53
0.087	3.49	5.89
0.092	3.72	4.10
0.094	5.675	6.583
0.1	6.6867	6.954

Table 7. Drag coefficient for the high roughness surfaces.

	Commercial name	
Velocity (m/s)	**P40**	**P80**
0.085	5.99	4.53
0.087	6.99	4.28
0.092	6.58	4.876
0.094	6.81	4.746
0.1	6.887	7.208

To calculate the Reynolds number we used kinematic viscosity of water which is 10^{-6} m^2/s.

Table 8. Reynolds number and its equivalent velocity.

Velocity (m/s)	**Reynolds number**
0.085	3400
0.087	3480
0.092	3680
0.094	3760
0.1	4000

After carrying out the experimental tests, a drag force was found, from an arithmetic mean of the force obtained in the 4 tests we managed to calculate mathematically the drag coefficient and velocities. As shown below the graphic of drag coefficient of the abrasive sheet P320 with different velocity, we can remark an augmentation for the Cd between the first velocity to the second and third and again another augmentation between the second and third to the fourth and fifth.

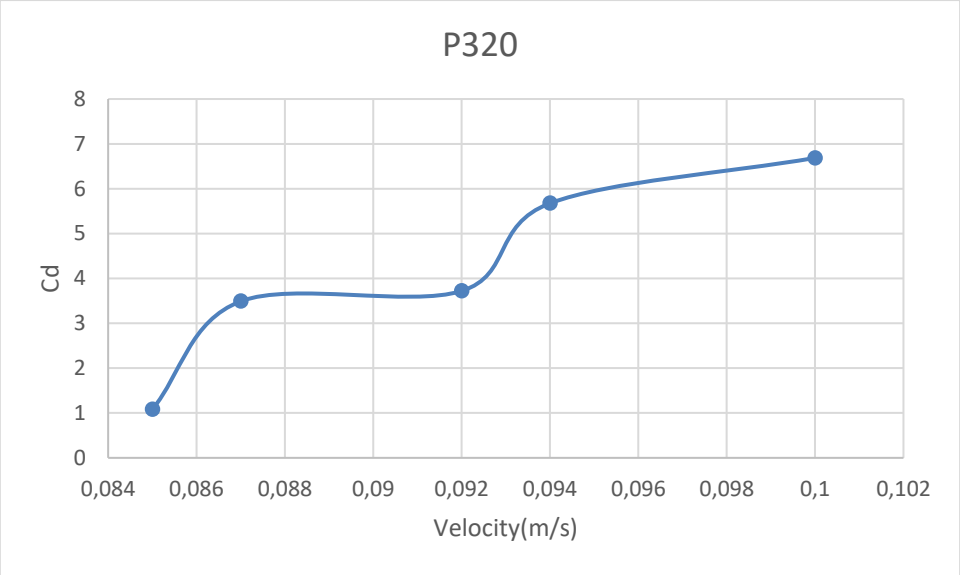

Figure 33. Drag coefficient of the abrasive sheet P320.

As shown below the graphic of drag coefficient of the abrasive sheet P120 with different velocities. We can see that it made a fall at the third velocity point and that might be due to the vibration of the water tunnel.

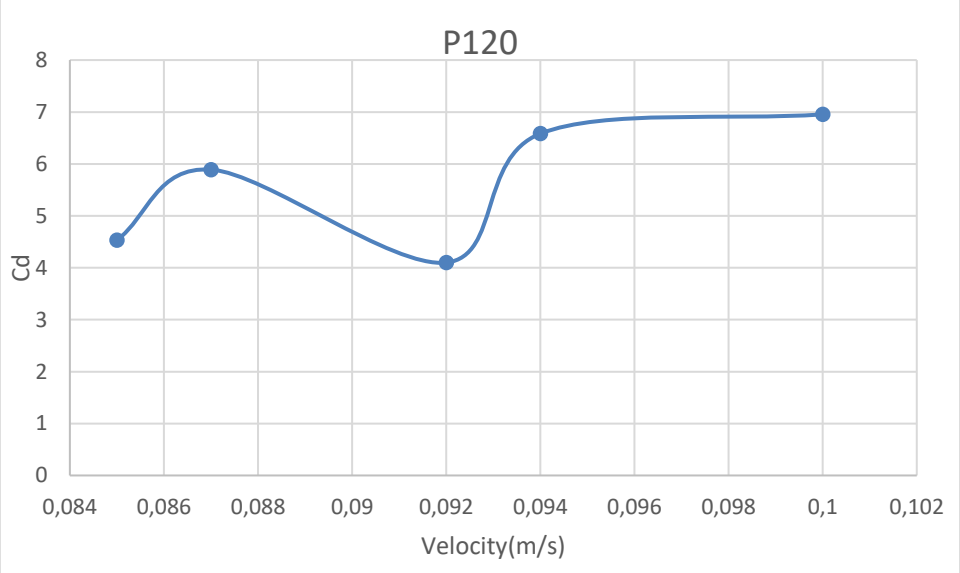

Figure 34.drag coefficient of the abrasive sheet P120.

As shown below the graphic of drag coefficient of the abrasive sheet P80 with different velocities. We remark that the curve started high and continued to augment with the velocity then it takes a little fall and then goes all the way up again

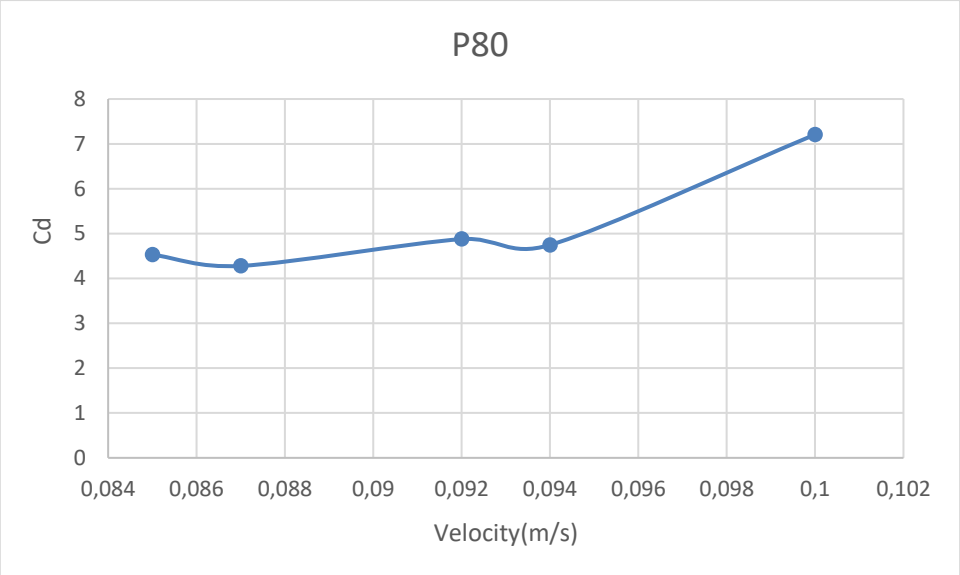

Figure 35. Drag coefficient of the abrasive sheet P80.

As shown below the graphic of drag coefficient of the abrasive sheet P40 with different velocities. We remark that the curve is almost linear.

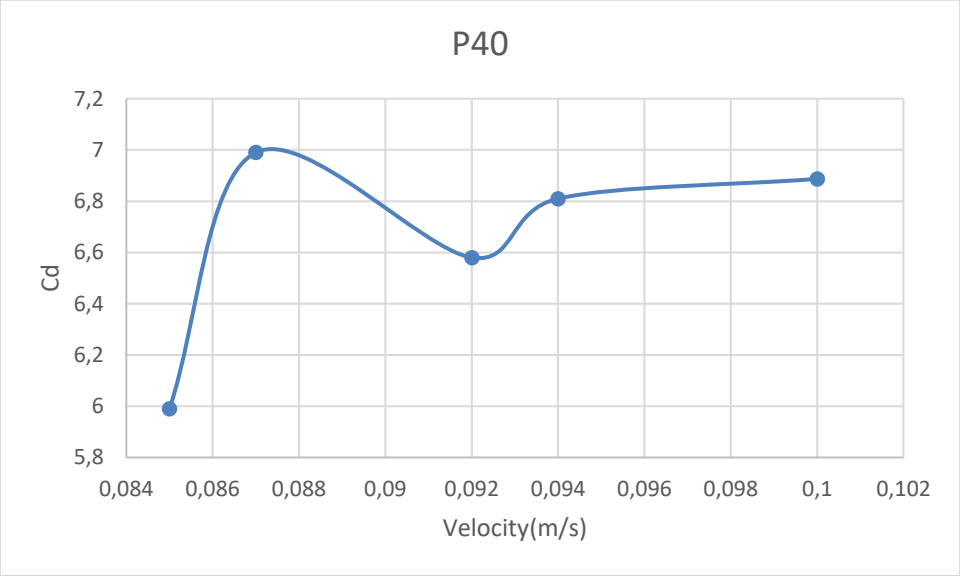

Figure 36. Drag coefficient of the abrasive sheet P40.

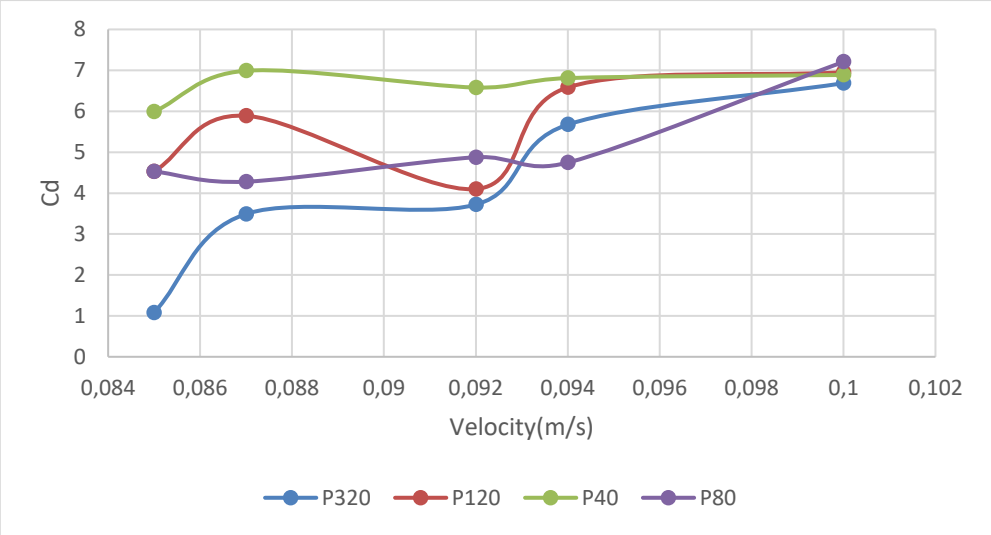

Figure 37. Drag coefficient of the abrasive sheets.

The previous graphs provide a fast comparison of drag forces in each model evaluated. When compared to smooth models, there were no significant differences in the values of forces when roughness was included.

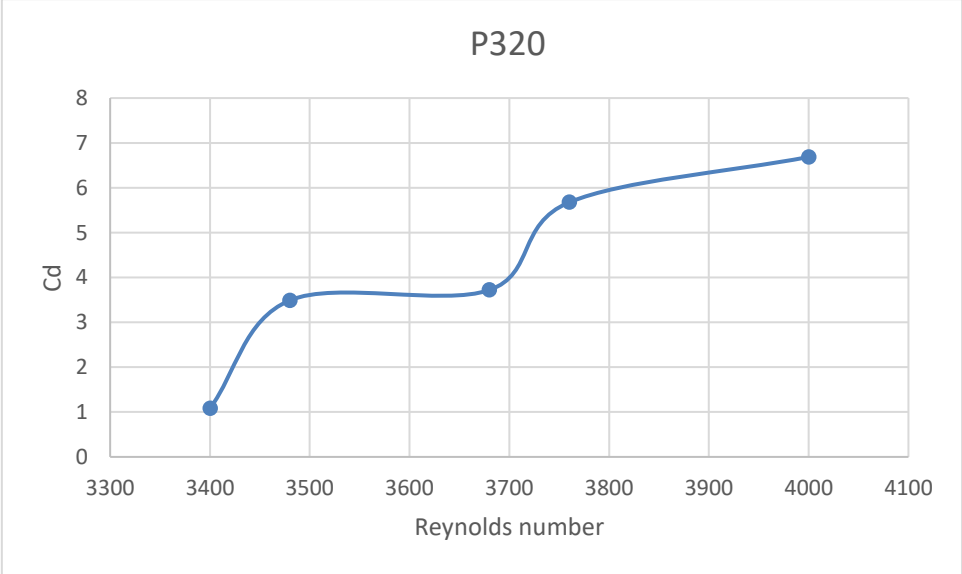

Figure 38. Drag coefficient of the abrasive sheet P320.

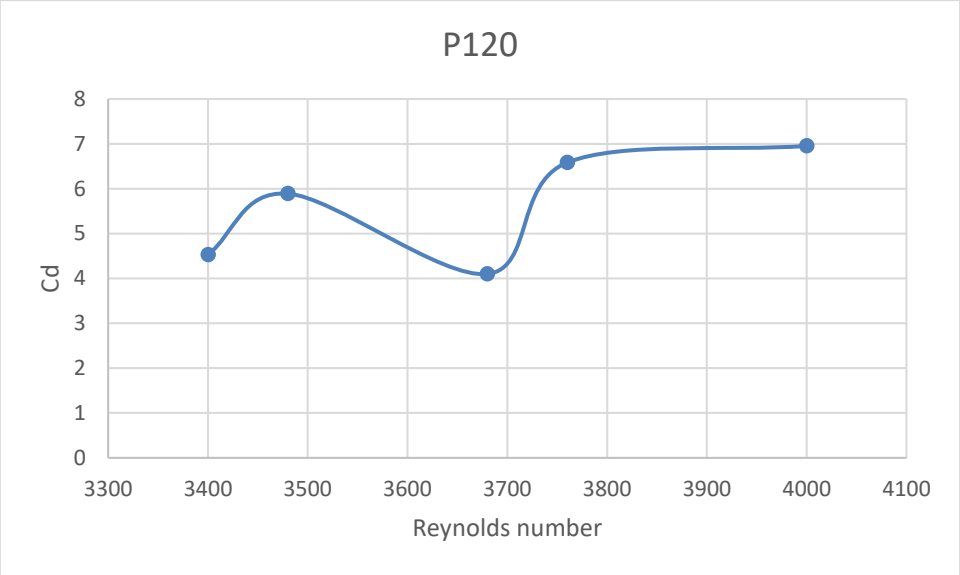

Figure 39. Drag coefficient of the abrasive sheet P120.

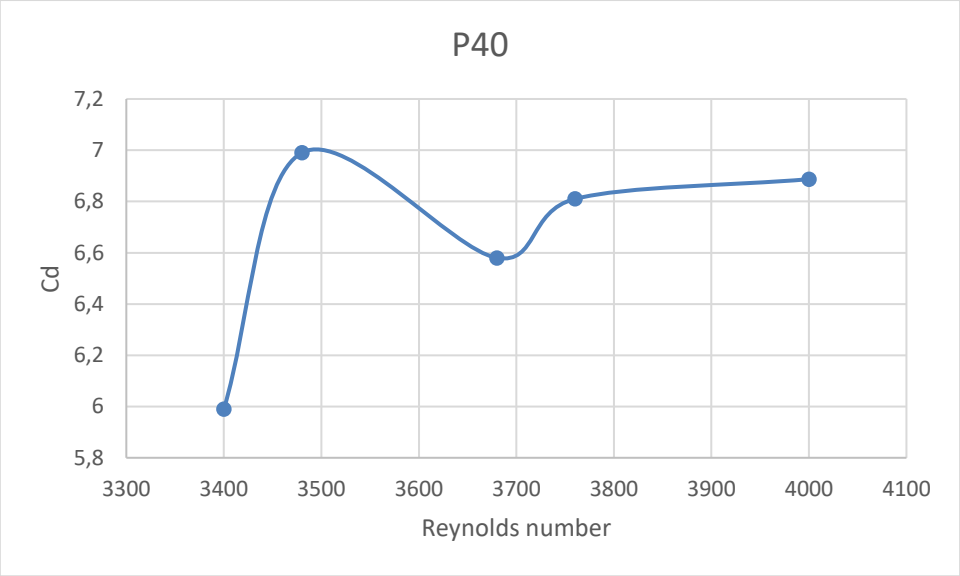

Figure 40. Drag coefficient of the abrasive sheet P40.

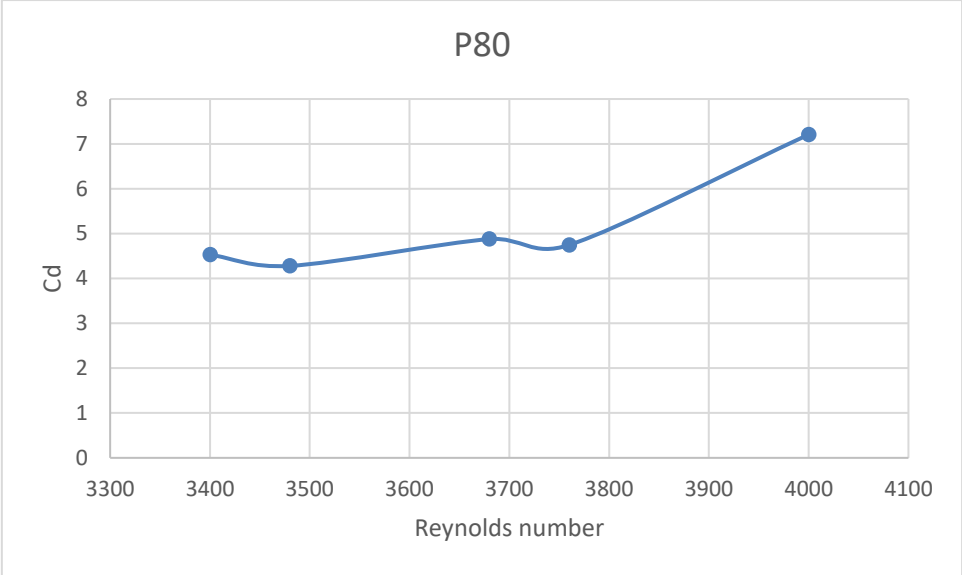

Figure 41. Drag coefficient of the abrasive sheet P80.

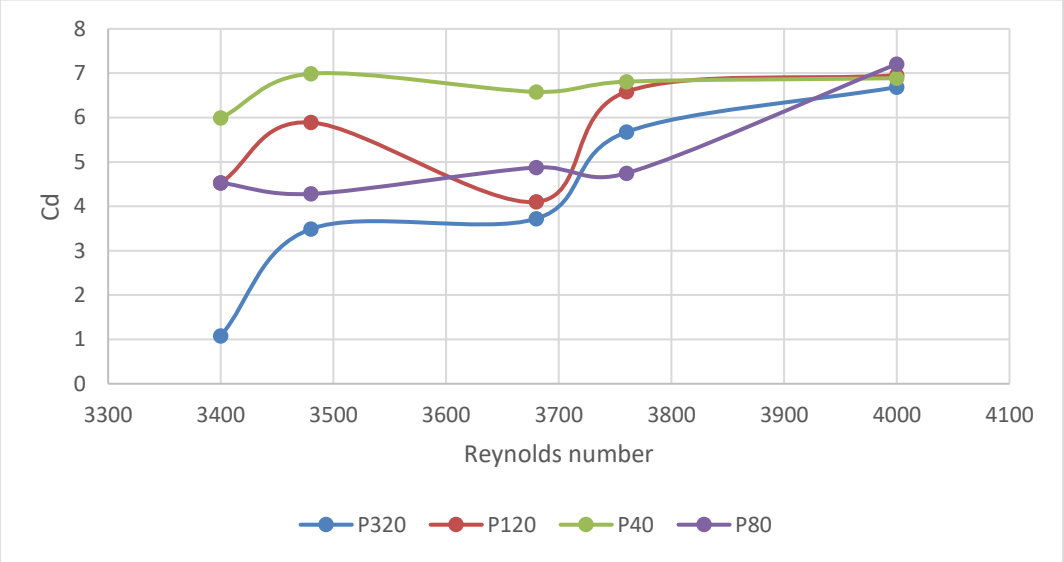

Figure 42. Drag coefficient of the abrasive sheets all together.

The previous graphs provide a fast comparison of drag forces of each model both separately and together, smooth models aren't that identical we can see the differences especially in the middle of the curves, while the rough ones have more in common.

CHAPTER 5

Conclusion

The results are objectively analyzed using comparing graphs, which aid in the visualization of behaviors while also guiding discussions. The first considerations include the force data (table 5) as well as the corresponding calculated drag coefficients (table 6) on smooth cylinders, as shown in the figures 33 and 34.

In the observation of the drag coefficients, as the relative roughness increased, the results show that the response to the insertion of roughness is an approximate expression of the behavior observed for the smooth model.

The Figures have considerable differences in drag coefficient, which may be seen visually. There were more variations in forces as the flow velocity increased, with the main extrapolations in the last force value obtained, which may have been due to the difficulty in keeping the measurement system stable and without vibrations at high speeds.

The cylinder's experimental findings were more quantitatively acceptable. Nevertheless, the data obtained from the resolution of the measurement system used explain the significant divergences in their respective drag coefficient, implying the need for a system that allows for force readings with more decimal places for a more reliable quantitative analysis in drag coefficient calculation. It's worth noting that the smallest percentage variances in force and drag coefficients were centered just before the speed range's center value, which can be seen when viewing their respective tables and the graphic behavior.

The introduction of abrasive sand paper resulted in different behaviors for the drag coefficients, which may be compared individually according to the varying relative roughness ε/D in the graphics.

Bibliographic references

[1] NUSSENZVEIG, M. Course in Basic Physics – vol. 2. 4th Edition. See. São Paulo: Blucher, 2002.

[2] WHITE, FM Fluid Mechanics. 7th edition. The McGraw-Hill Companies, New York, NY, 2011. ISBN 978-0-07-352934-9.

[3] ÇENGEL, YA; CIMBALA, JM Fluid Mechanics: Fundamentals and Applications. The McGraw-Hill Companies, New York, NY, 2006. ISBN 0-07-247236-7.

[4] VISCOSYMETERS.TOP. Ostwald viscometers. 2021. Available at < https://viscosimeters.top/viscosimeters-ostwald/ > Access in 3rd September 2021.

[5] FONTANA, E. Determination of Viscosity of Newtonian Fluids. Notes on Transport Phenomena. Federal University of Santa Catarina – UFSC. Available at < https://fontana.paginas.ufsc.br/disciplinas/fenomenos-experimental-i/> Access in 3rd September 2021.

[6] PRITCHARD, PJ; LEYLEGIAN JC; Fox and McDonald's Introduction to Fluid Mechanics. 8th edition. John Wiley & Sons, Inc.2011. ISBN 13 9780470547557 and ISBN-10 0470547553

[7] ANSHUMAN SHRIVASTAVA. Introduction to Plastics Engineering.2018. Available at < https://www.sciencedirect.com/topics/engineering/rheometer > Access in 4th September 2021.

[8] PRAVATO, W. Study of aerodynamic drag from wind tunnel simulations. Final dissertation report presented to the Superior School of Technology and Management to obtain the Master's degree in Industrial Engineering. 2020. Available at< https://bibliotecadigital.ipb.pt/bitstream/10198/22679/1/pauta-relatorio-29.pdf > Access in 10th September 2021

[9] BRUNETTI, F. Fluid mechanics. 2nd Edition. Rev. São Paulo: Pearson Prentice Hall, 2013.

ISBN 978-85-212-0299-8.

[10] SCHLICHTING, H.; GERSTEN, K. Boundary-Layer Theory. Physics and astronomy. Springer, 2000.

[11] ANDERSON JR, JD Fundamentals of aerodynamics. 5th edition. The McGraw-Hill Companies, New York, NY, 2010. ISBN 978-0-07-339810-5.

[12] NATIONAL AERONAUTICS AND SPACE ADMINISTRATION. Reynolds Number. Available at: <https://www.grc.nasa.gov/www/k-12/airplane/reynolds.html>. Access in 3rd September 2021.

[13] CHANSON, H. The hydraulics of open channel flow: an introduction. 2nd Edition. Elsevier Butterworth-Heinemann. 2004. ISBN 0-7506-5978-5.

[14] CLAUDINO, D. Design and dimensioning of a canoe – drag measurement. Final Project Work Report presented to the Superior School of Technology and Management - Polytechnic Institute of Bragança. 2019. Available at < https://bibliotecadigital.ipb.pt/bitstream/10198/19535/1/pauta-relatorio-14.pdf > Access in 10th September 2021

[15] GUNT HAMBURG. Equipment for Engineering Education. Available at < https://www.gunt.de/en/products/visualisation-of-streamlines-in-an-open-channel/070.15021/hm150-21/glct-1:pa-148:pr-568 > Access in September 13th. 2021

[16] ENGINEERING LABORATORY DESIGN. Hydraulic Channels. Available at < http://www.eldinc.com/hydraulic-channels > Access in 8th September. 2021

[17] AZO MATERIALS. Rheometers: How and What do they Measure? .2021. Available at < https://www.azom.com/article.aspx?ArticleID=18927 > Access in 2nd September 2021.

[18] STEVEN J. SHIRE. he molecular basis of high viscosity of monoclonal antibodies at high concentration. Woodhead Publishing 2015. ISBN 9780081002964. 2015. Available at <

https://www.sciencedirect.com/science/article/pii/B9780081002964000099 > Access in 4th September 2021.

[19] SILVA, V. COSTA, M. Influence of Processing on Rheological and Texturel Characteristics of Goat and Sheep Milk Beverages and Methods of Analysis. 2019. Available at <https://www.sciencedirect.com/science/article/pii/B9780128152591000112> Access in 4th September 2021.

[20] DIAS, V. Determination of The Drag Coefficient of an Autonomous Solar Lighting Column Using Wind Tunnel Simulation and Computational Analysis. Dissertation presented to Higher School of Technology and Management Polytechnic Institute of Bragança to obtain the master's degree at Industrial Engineering. 2019. Available at < https://bibliotecadigital.ipb.pt/handle/10198/20519 > Access in 11 September 2021.